Progr Colloid Polym Sci (2004) 128: 113–119
DOI 10.1007/b97103

Alexsandro Santos Costa
Toyoko Imae
Katsuhiko Takagi
Koichi Kikuta

Intercalation of dendrimers in the interlayer of hydrotalcite clay sheets

Abstract Nanocomposites have been prepared through the intercalation of poly(amido amine) dendrimers with carboxylate terminals into hydrotalcite clays. The formation of nanocomposites by anion exchange during incubating at 70 °C was investigated at various compositions with increasing dendrimer content in water and was assessed by Fourier transform IR absorption spectroscopy, X-ray diffraction, small-angle X-ray scattering, and elemental analysis. The dendrimer diffused into the clay galleries: the spacing between the clay layers (sheets) increased from its intrinsic value of 3.2 to 20–23 Å, and the mass fraction of the dendrimer in the composite was around 0.50 for mixing ratios (charge of clay to carboxylate of the dendrimer) higher than 1:2, indicating the saturated intercalation of the dendrimer in the clay. The dendrimers are densely packed with an ellipsoidal structure in the interlayer. At a mixing ratio of 1:8, there was excess adsorption of the dendrimer on the clay surface besides the intercalation and initial adsorption.

A. Santos Costa · T. Imae
Graduate School of Science,
Nagoya University, Chikusa,
Nagoya 464-8602

T. Imae (✉)
Research Center for Materials
Science, Nagoya University,
Chikusa, Nagoya 464–8602, Japan
e-mail: imae@nano.chem.nagoya-u.ac.jp
Tel.: +81-52-7895911
Fax: +81-52-7895912

K. Takagi, K. Kikuta
Graduate School of Engineering,
Nagoya University, Chikusa,
Nagoya 464-8603, Japan

Keywords Poly(amido amine) dendrimer · Hydrotalcite · Clay · Intercalation · X-ray diffractometry

Introduction

Dendrimers [1] are highly branched macromolecules consisting of a multifunctional core, to which repeating units are sequentially covalently bonded to create a topologically regular structure. The resultant molecules present a well-defined number of terminal groups and a narrow molecular weight distribution that is truly monodisperse in most cases. Owing to their structural uniformity, dendrimers provide a valuable model for correlating the macromolecular structure to the technological function [2–5]. Thus, dendrimers have a wide range of applications, including drug delivery [6], catalysis, and sensors [7–8] in high-technology fields. The organization of dendrimers in monolayers results in materials that can be applied as devices [7–10] and scaffolds for posterior elaborations [11–17]. Moreover, stratumous-layered composites of a dendrimer and a linear polymer can be prepared by linking terminal groups of a dendrimer to functional groups of a polymer [12, 13, 16, 18–20].

Double-layered hydroxides, also known as ionic clays, are important inorganic materials, and have deserved

much attention in recent years. The hydrotalcite is constituted from inorganic sheets that are similar to the basic structure of brucite, $Mg(OH)_2$ [21]. The brucite-like sheets become positively charged owing to the partial substitution of divalent metal cations by trivalent metal cations in the layer structure. In order to balance the extra charges developed by the trivalent cations and to maintain electrical neutrality, organic or inorganic anions and water molecules are intercalated between the interlayer of the clay. Anions like Cl^- and CO_3^{2-} existing in the crude clay can be easily replaced by many other molecules, depending on their charge affinity. The anion-exchange properties of hydrotalcite [22] have been explored for the intercalation of long-chain fatty acids [23], organic dyes [24], phthalocyanine-type molecules [25, 26], aromatic ketocarbonates [27], etc. Intercalation of large anions has also been tried, and the successful intercalation of oxymetalates and phthalocyanines has been reported [28, 29]. The interest in these composites lies in their potential and technological functionality as catalysts or catalyst supports [21], anion adsorbents [30], medicine stabilizers [31], ion exchangers [32], for controlled release of anions [33], and as components of ceramic-based nanocomposites [21].

To date no one has reported the use of a clay framework for the fabrication of dendrimer stratums. Here, we report a new approach to obtain organic/inorganic multilayered nanocomposites making use of a dendrimer and a clay. We investigated the formation of nanocomposites through the intercalation of a dendrimer in the clay interlayer. The structure of the nanocomposites was studied regarding the preservation of the original structural organization of the clay as well as changes of interlayer distance and dendrimer conformation. The poly(amido amine) (PAMAM) dendrimer with carboxylate terminals used in this study is negatively charged in water. Such charges act as the driving force in the anion-exchange process in the hydrotalcite clay. A 4.5th generation (G4.5) dendrimer was used to promote considerable change in the hydrotalcite interlayer spacing. Nanocomposites were prepared at high temperature to assist the hydrotalcite swelling and to facilitate the dendrimer diffusion into the clay interlayer. The preparation of nanocomposites was investigated at different hydrotalcite/dendrimer ratios. In order to assess the intercalation, the structural changes were monitored by X-ray diffraction (XRD) and small-angle X-ray scattering (SAXS). Furthermore, we discuss the packing and the structure of the dendrimer in the nanocomposites at different ratios assessed by X-ray diffraction and elemental analysis. Two-dimensional organization of dendrimers by using clay as a platform should be utilizable in the preparation of dendrimer-containing nanocomposites that are applicable to systems of drug-delivery, catalysis, sensors, and so on.

Experimental

Materials

Hydrotalcite clay, $[Mg_{4.5}Al_2(OH)_{13}Cl_2]\cdot 3.5H_2O$, was donated from Kyowa Chemical Co. and was used as received. Its anion-exchange capacity is 350mEq 100 g^{-1}. The G4.5 PAMAM dendrimer with carboxyl terminal groups (molecular weight 26,258, 128 terminal groups) was purchased from Aldrich and was used as received. MilliQ water was used throughout the experiment.

Nanocomposite preparation

PAMAM dendrimer was dried by purging it with nitrogen for 1 h and then by drying it in vacuo for 30 min. Water and hydrotalcite clay were added to the dendrimer residue in order to prepare hydrotalcite/PAMAM dendrimer mixtures at different ratios. The composition number ratio (anionic charge of clay to carboxylate of the dendrimer) varied from 1:1 to 1:8, where the clay concentration was kept constant. The mixtures were incubated at 70 °C for 24 h under shaking, where the adsorption equilibrium is attained. The resulting materials were filtered using a Millipore filter (0.22 μm pore size), washed a few times with water to remove the possible excess of free dendrimer, and dried.

Measurements

Fourier transform IR (FT-IR) spectra were acquired by using a Bio-Rad FTS 575C FT-IR spectrometer in the range 1,000–4,000 cm^{-1} at 4-cm^{-1} resolution. A few milligrams of hydrotalcite/PAMAM mixtures or hydrotalcite were ground with potassium bromide and afterwards pressed to prepare discs. The spectrum of a dendrimer was measured by dropping a small volume of a dendrimer solution in methanol onto a pure KBr disc.

The XRD patterns were recorded using a Rigaku RINT 2100 V X-ray diffractometer possessing Cu Kα radiation of wavelength 1.54 Å, operating at 60 kV and 50 mA and scanning at a rate of 0.5° min^{-1}.

SAXS measurements were performed with a Rigaku instrument (SAX-LPB), equipped with an ultraX18HB X-ray source and He-protected CMF25-77.5Cu6 confocal multilayer optics. The radiation used was Cu Kα ($\lambda = 1.54$ Å) and the supply voltage and current were 45 kV and 60 mA, respectively. Prior to the measurements, specimens were placed between two Kapton films and dried at 60 °C for a few minutes. Two-dimensional SAXS patterns were recorded on a Fuji imaging plate (13×13 cm^2) detector. The sample-to-detector distance was set to 0.5 m and the exposure time to 24 h. Scanned scattering patterns were azimuthally averaged and corrected for a background of two Kapton films in the air gap. The scattering function $I(2\theta)$ was converted to $I(q)$, where 2θ is the scattering angle and $q = 4\pi\sin(2\theta/2)/\lambda$ is the scalar of the scattering vector.

Elemental analysis experiments were done using a LECO CHN-900 C, H, N analyzer. Prior to the analysis, mixtures were dried in vacuo in a desiccator containing P_2O_5 for 16 h.

Results

FT-IR spectra and band assignment of the hydrotalcite, dendrimer, and mixtures of hydrotalcite/dendrimer are presented in Fig. 1 and Table 1, respectively. The hydrotalcite spectrum showed a broad absorption band at 3,474 cm^{-1} which is attributed to an OH stretching vibration mode of intercalated and adsorbed water

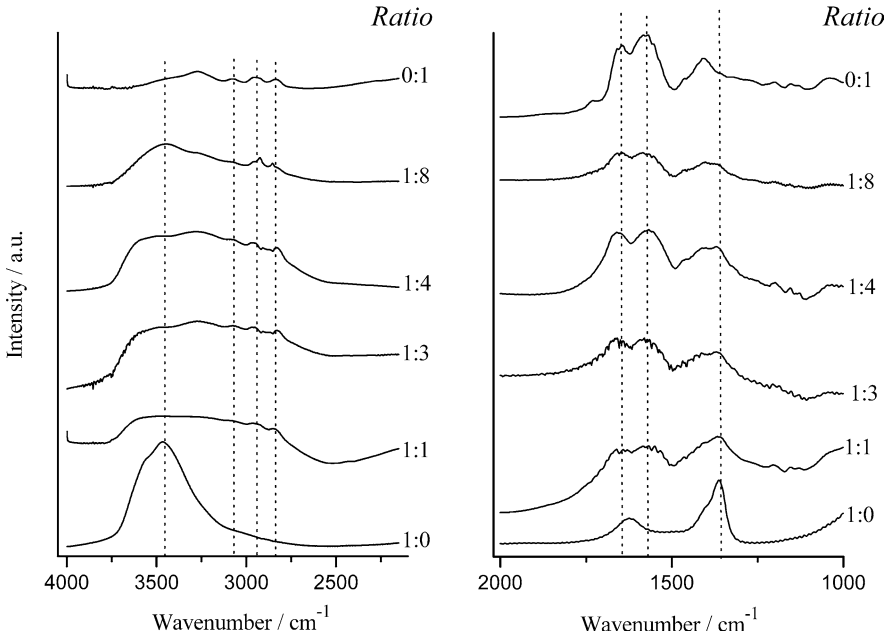

Fig. 1 Fourier transform IR spectra for mixtures at different mixing ratios of hydrotalcite to dendrimer

molecules and/or the hydroxyl groups of brucite-like sheets [34–39]. In addition to this band, the spectrum of hydrotalcite showed an absorption band at 1,624 cm^{-1} assigned to a HOH bending mode. The absorption band at 1,364 cm^{-1} is attributed to carbonate anion impurities [40, 41]. The carbonate anions have high affinity for hydrotalcite cations. Hence, Cl anions are easily replaced with carbonate anions in the hydrotalcite interlayer during the synthesis or the dispersion of hydrotalcite in water.

The FT-IR spectra of all hydrotalcite/dendrimer mixtures displayed very broad absorption bands between 3,700 and 3,300 cm^{-1}, which coincide with the broad IR band of OH groups in hydrotalcite. A HOH bending band of hydrotalcite is not observed in the spectra of the mixtures and this may be caused by the superposition with dendrimer bands or the shift of the HOH band. The band of the carbonate anion impurities shifts to 1,370 cm^{-1} with increasing fraction of the dendrimer in the mixture. The hydrotalcite/dendrimer mixtures also displayed absorption bands that are associated with the dendrimer, as is apparent when comparing the IR spectrum with the IR spectrum of the G4.5 PAMAM dendrimer [42]. The bands at 3,275, 3,078, 2,957, and 2,833 cm^{-1} represent the amide A and B (NH stretching mode) and CH_2 antisymmetric and symmetric stretching

Table 1 Assignments of IR absorption bands of hydrotalcite, dendrimer, and the hydrotalcite/dendrimer mixture. Spectral resolution 4 cm^{-1}

Assignment	Band position/cm^{-1}[a]		
	Hydrotalcite	Dendrimer	Hydrotalcite/dendrimer mixture
OH stretching	3,474(b, s)		3,482(b, s)
Amide A (NH stretching)		3,272(s)	3,275(s)
Amide B (NH stretching)		3,077(m)	3,078(m)
CH_2 antisymmetric stretching		2,957(m)	2,957(m)
CH_2 symmetric stretching		2,834(m)	2,833(m)
C=O stretching		1,730(m)	1,731(w)
Amide I		1,643(vs)	1,645(vs)
HOH bending	1,624(m)		–
COO^- antisymmetric stretching		1,584(vs)	1,585(vs)
Amide II		1,570(vs)	1,572(vs)
COO^- symmetric stretching		1,406(s)	1,407(s)
CO_3^{2-} (impurity)	1,364(vs)		1,370(m)
Amide III		1,358(w)	1,360(w)
C–N stretching		1,040(w)	1,048(w)

a) (vs) very strong, (s) strong, (m) medium, (w) weak, (b) broad

modes, respectively, and originated from the PAMAM dendrimer. The absorption bands at 1,731, 1,645, 1,585, 1,572, and 1,407cm^{-1} are attributed to the C=O stretching, amide I, COO^- antisymmetric stretching, amide II, and COO^- symmetric stretching modes, respectively. The bands at 1,360 and 1,048 cm^{-1} were assigned to the amide III and C–N stretching. The presence of IR bands of the PAMAM dendrimer in the specimens after rinsing indicates the complex formation between hydrotalcite and the PAMAM dendrimer. It should be noted that the intensity ratio between the IR bands of carbonate anion impurities and the dendrimer is almost constant at a mixing ratio above 1:2.

Information on the morphology and crystallinity were obtained from analysis of XRD data. The XRD patterns and the indexing of the hydrotalcite and hydrotalcite/dendrimer mixtures are shown in Fig. 2 and Table 2, respectively. The spectra are shown as $I(q)\times q^2$ versus q (Kratky representation). The spacing between the reflection planes was calculated from the indexed Bragg peak position q_{hkl}, where hkl are the Miller indices, and from the equation $dhkl = 2\pi/qhkl$. Typically, the XRD pattern of hydrotalcite presents major diffraction peaks: (1) the large basal spacing (d_{003}); (2) the half-height harmonic spacing (d_{006}) (where $d_{006} = d_{003}/2$); and (3) the d_{009} diffraction (where $d_{009} = d_{003}/3$) [43]. The hydrotalcite spectrum, as seen in Fig. 2, exhibits strong and sharp diffraction peaks at $q = 0.788$, 1.600 and 2.440 Å^{-1}, which correspond to a basal spacing (d_{003}) value of 7.97 Å. The thickness (4.77 Å) of the brucite-like sheet [44] is a good approximation of the thickness of a single $Mg^{\cdots}Al^{\cdots}(OH)_x$ (hydrotalcite) layer. Subsequently, the interlayer distance is simply found by subtracting 4.77 Å from the observed basal spacing. In this case, the interlayer distance was 3.20 Å, which correlates well with the size of the foremost-entrapped anion, Cl^-. All hydrotalcite/dendrimer mixtures present, in addition to the diffraction peaks of the crude hydrotalcite, new diffraction peaks around $q = \sim 0.23$ Å^{-1} and $q = \sim 0.52$ Å^{-1} at mixing ratios larger than 1:1. The new peaks are indexed as the dendrimer intercalated spacing (d_{003}),

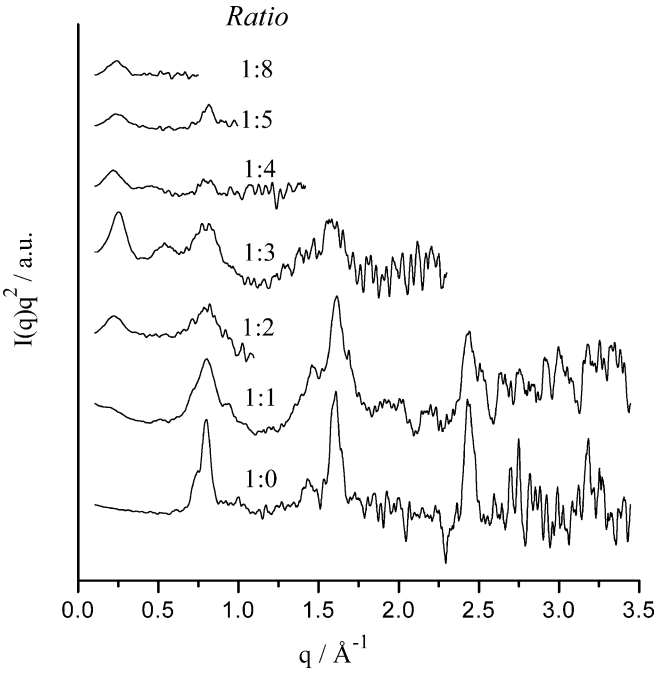

Fig. 2 X-ray diffraction patterns for mixtures at different mixing ratios of hydrotalcite to dendrimer

Table 2 Bragg peak positions (Å^{-1}) for mixtures at different ratios, with the indexes according to rhombohedral R(-3)m symmetry in *parentheses*, and data evaluated from Bragg peaks

Ratio	Basal hydrotalcite	Dendrimer-intercalated hydrotalcite	Dendrimer layer thicknessÅ	Area occupied by dendrimer/Å^2
1:0	0.788 (003)			
	1.600 (006)			
	2.440 (009)			
1:1	0.788 (003)			
	1.607 (006)			
	2.420 (009)			
1:2		0.230 (003)		
	0.790 (003)	–		
1:3		0.250 (003)		
		0.530 (006)		
	0.800 (003)	–	20.4	7.92×10^3
	1.600 (006)	–		
1:4		0.224 (003)		
		0.480 (006)	23.3	6.93×10^3
	0.810 (003)	–		
1:5		0.245 (003)		
		0.520 (006)	20.9	7.73×10^3
	0.820 (003)	–		
1:8		0.240 (003)		
		0.530 (006)	21.4	7.57×10^3

which is around 25–28 Å. The coexistence of diffraction peaks of crude hydrotalcite suggests that there are interlayers in which the Cl^- anions were not replaced by the dendrimer molecules.

To obtain more information on the character of hydrotalcite/dendrimer systems, SAXS measurement was performed and scattering patterns were plotted as $I(q)$ versus q (Fig. 3). The crude hydrotalcite presented no reflection peak, since the basal distances for hydrotalcite intercalated with Cl^- and CO_3^{2-} anions give reflections outside the measured q range in SAXS. Hydrotalcite/dendrimer mixtures prepared at ratios of 1:2–1 T:8 showed broad bands at 0.224–0.250 and 0.480–0.530 $Å^{-1}$, which are the interlayer spacings d_{003} and d_{006} for hydrotalcite intercalated by dendrimer molecules.

Elemental analysis was used to assess the dendrimer content in the hydrotalcite/dendrimer mixtures. Since nitrogen atoms are nonexistent in the hydrotalcite structure, the dendrimer mass fraction, f_D, was calculated directly from the N content in the hydrotalcite/dendrimer mixture, as listed in Table 3, which also includes the results of elemental analysis. Mixtures at ratios of 1:3, 1:4, and 1:5 presented very similar results, where the fraction was constant at 0.495. This numerical value indicates that the dendrimers are almost fully intercalated in the interlayer of the clay and are adsorbed on the surface of the clay. On the other hand, the mixture at a ratio of 1:8 presented a higher fraction (0.558) of dendrimers. This may be due to the additional (excess) adsorption of dendrimers on the adlayer of the dendrimer on the surface of the clay.

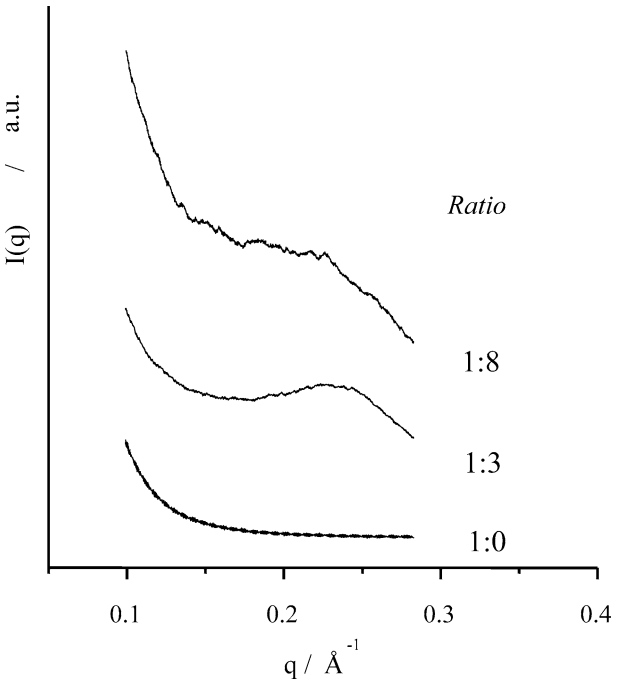

Fig. 3 Small-angle X-ray scattering patterns for mixtures at different mixing ratios of hydrotalcite to dendrimer

Discussion

To ensure the intercalation of the dendrimer into hydrotalcite, the hydrotalcite/dendrimer mixtures were incubated at high temperatures. The IR results evidenced the complex formation after the incubation. There are two possible ways of hydrotalcite/dendrimer composite formation: the intercalation of the dendrimer into hydrotalcite and its adsorption onto hydrotalcite. The X-ray techniques were used to study the morphology of dendrimer/hydrotalcite mixtures. XRD and SAXS indicated that dendrimer molecules were intercalated into hydrotalcite. The lamellar structure is preserved upon the intercalation of the dendrimer but the interlayer distance increased, as illustrated in Fig. 4.

At first glance, the XRD spectra seemed to be similar but some trends were observed with an increase in the

Table 3 Elemental analysis results for mixtures at different ratios and data evaluated from elemental analysis

Ratio		C/wt %	H/wt %	N/wt %	Dendrimer mass fraction f_D	Hydrotalcite area per dendrimer/$Å^2$
1:3	Observed	22.56	5.56	7.22	0.495 ± 008	1.73×10^3
	Calculated using f_D	22.77	3.09	6.60		
1:4	Observed	22.55	5.72	7.17	0.495 ± 0.006	1.73×10^3
	Calculated using f_D	22.78	3.09	6.60		
1:5	Observed	22.66	5.64	6.69	0.494 ± 0.009	1.74×10^3
	Calculated using f_D	22.73	3.08	6.59		
1:8	Observed	25.82	5.57	7.39	0.558 ± 0.004	1.35×10^3
	Calculated using f_D	25.70	3.49	7.45		

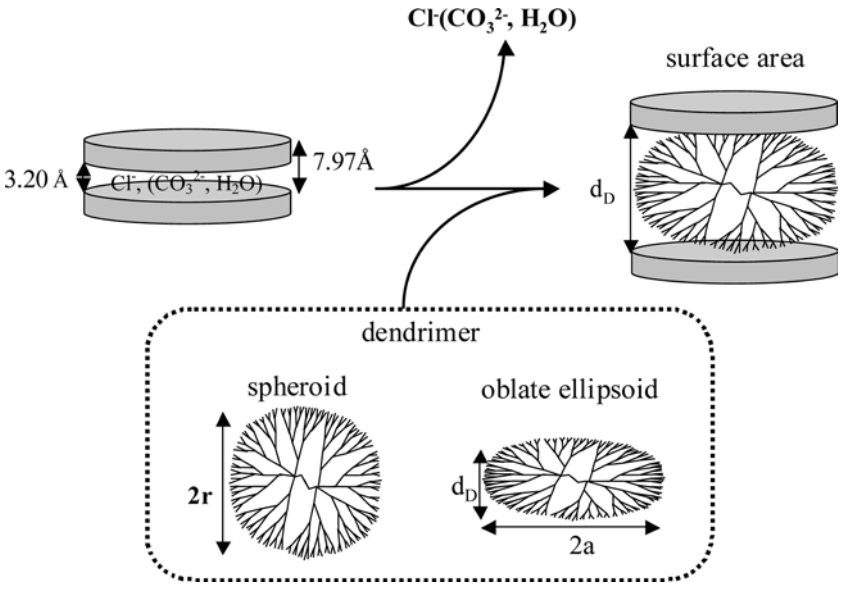

Fig. 4 Schematic representation of a dendrimer intercalated into hydrotalcite via direct ion exchange

amount of dendrimer in the mixtures. The diffraction peak of the basal spacing of dendrimer-intercalated hydrotalcite dispersed within 0.22–0.25 $Å^{-1}$ at mixing ratios of 1:2–1:8, indicating the saturation of intercalation. On the other hand, there was a progressive increase from 0.79 to 0.82 $Å^{-1}$ in the diffraction peak position corresponding to the basal distance of the crude hydrotalcite. These positions coincide with the spacing of hydrotalcite that interlaid Cl^- (7.9 Å) and CO_3^{2-} (7.6 Å), respectively [45]. The carbonate anions are strongly adsorbed on hydrotalcite and/or intercalated in it, as revealed by IR spectroscopy. On the basis of these facts, it was proposed that, even at higher mixing ratios, there are some regions of hydrotalcite intercalated with mainly carbonate anions and possibly chloride anions.

Although the diameter of the spherical G4.5 PAMAM dendrimer is around 59 Å [46], the hydrotalcite interlayer intercalated with dendrimer molecules was not thicker than 24 Å. Dendrimer molecules of lower generation are flexible rather than hard and spherical. This indicates that dendrimer molecules distort their shape from a sphere, when intercalated into hydrotalcite. Similar distortion of the dendrimer structure was observed between lamellar bilayers of didodecyldimethylammonium [47].

The area occupied by a dendrimer molecule was evaluated by making use of the XRD results. The dendrimer in solution presents a spherical shape with a diameter represented by $2r$ (59 Å for the G4.5 PAMAM dendrimer) [46]. On the other hand, from the basal distance obtained from the XRD results, we assume that the dendrimer molecules are intercalated with an oblate ellipsoidal structure. If the volume of the dendrimer does not change during the structural deformation, the volume obtained for the spheroid shape can be matched to that of an oblate ellipsoid in order to obtain the long-axis diameter of the dendrimer denoted as $2a$ in Fig. 4. The dendrimer layer thickness, d_D, that was obtained from the XRD result and that is listed in Table 2 was used as the short-axis diameter in the oblate ellipsoid. Then, the spheroid volume of $(4/3)\pi r^3$ is equal to the oblate ellipsoid volume of $(4/3)\pi a^2(d_D/2)$. Making use of the evaluated long-axis diameter $2a$ of the intercalated dendrimer, we obtained the area (πa^2) occupied by a dendrimer molecule, which is listed in Table 2.

The dendrimer packing within the interlayer of hydrotalcite clay was also studied by making use of the result of elemental analysis and was compared with the intercalation structure obtained from XRD. In this study, a model where all interlayers are intercalated with dendrimer molecules was used, even though the coexistence of chloride and carbonate anions with dendrimers in the hydrotalcite interlayer is more likely to be true from the XRD results. From the combination of the dendrimer mass fraction f_D, obtained from elemental analysis, the clay area (50.6 $Å^2$) [47] per charge site and the anionic exchange capacity (350 mEq 100 g^{-1}), we calculated the hydrotalcite area per dendrimer $[50.6\times350\times10^{-3}\times N_A(1-f_D)/2]/(f_D N_A\times100/M_{den})$, where N_A is the Avogadro number and M_{den} (26,258) is the molecular weight of the PAMAM dendrimer. The hydrotalcite area per molecule, which is listed in Table 3, was smaller than the area occupied by the dendrimer obtained from XRD (Table 2). This discrepancy may occur because (1) the intercalated dendrimers coexist with the intercalated chloride and carbonate anions in the clay interlayer, (2) dendrimer molecules are not only intercalated in the clay interlayer but are also adsorbed

on the clay surfaces, or (3) the intercalated dendrimers are overlapped or compressed.

Conclusions

We have prepared nanocomposites composed of a clay and a dendrimer through the intercalation of a PAMAM dendrimer into the interlayer of hydrotalcite clay. The XRD and SAXS results of nanocomposites indicated the increase of the clay interlayer distance after the intercalation. The saturation of dendrimer intercalation was also identified, and the possible dendrimer adsorption on the hydrotalcite clay was assumed. The nanocomposites obtained may be useful as dendrimer storage systems and in processes where dendrimer-controlled release is desirable.

References

1. Tomalia DA, Baker H, Dewald J, Hall M, Kallos G, Martin S, Roeck J, Ryder J, Smith P (1985) Polym J 17:117–132
2. Nagasaki T, Ukon M, Arimori S, Shinkai S (1992) J Chem Soc Chem Commun 608–610
3. Nagasaki T, Kimura O, Ukon M, Arimori S, Hamachi I, Shinkai S (1994) J Chem Soc Perkin Trans 1 75–81
4. Jansen JFGA, de Brabander-van den Berg EMM, Meijer EW (1994) Science 266:1226–1229
5. Jansen JFGA, Janssen RAJ, de Brabander-van den Berg EMM, Meijer EW (1995) Adv Mater 7:561–564
6. Esfand R, Tomalia DA (2001) Drug Discovery Today 6:427–436
7. Wells M, Crooks, RM (1996) J Am Chem Soc 118:3988–3989
8. Tokuhisa H, Crooks RM (1997) Langmuir 13:5608–5612
9. Losada J, Cuadrado I, Moran M, Casado, CM, Alonso B, Barranco M (1997) Anal Chim Acta 338:191–198
10. Koo BW, Song CK, Kim C (2001) Sens Actuators B 77:432–436
11. Watanabe S, Regen, SL (1994) J Am Chem Soc 116:8855–8856
12. Zhou Y, Bruening ML, Bergbreiter DE, Crooks RM, Wells MJ (1996) J Am Chem Soc 118:3773–3774
13. Liu Y, Bruening ML, Bergbreiter DE, Crooks RM (1997) Angew Chem Int Ed Engl 36:2114–2116
14. Tsuruk VV, Rinderspacher F, Bliznyuk VN (1997) Langmuir 13:2171–2176
15. Tsuruk VV (1998) Adv Mater 10:253–257
16. Zhao M, Liu Y, Crooks RM, Bergbreiter DE (1999) J Am Chem Soc 121:923–930
17. Wang J, Chen J, Jia X, Cao W, Li M (2000) Chem Commun 511–512
18. Grohn F, Kim G, Bauer BJ, Amis EJ (2001) Macromolecules 34:2179–2185.
19. Sellner H, Karjalainen JK, Seebach D (2001) Chem Eur J 7:2873–2887
20. Alvarez J, Sun L, Crooks RM (2002) Chem Mater 14:3995–4001
21. Cavani F, Trifiro F, Vaccari A (1991) Catal Today 11:173–301
22. Allmann R (1970) Chimia 24:99–108
23. Raki L, Rancourt DG, Detellier C (1995) Chem Mater 7:221
24. Park IY, Kurado K, Kato C (1990) J Chem Soc Dalton Trans 3071
25. Carrado KA, Forman JE, Botto RE, Winans RE (1993) Chem Mater 5:472
26. Bonnet S, Forano C, de Roy D, Besse JP, Millard P, Momenteau M (1996) Chem Mater 8:1962
27. Takagi K, Harata E, Shicchi T, Kanoh T, Sawaki Y (1997) J Photochem Photobiol 105:47–54
28. Gardner EA, Yun SK, Kwon T, Pinnavaia TJ (1998) Appl Clay Sci 13:479–494
29. Chatti I, Ghorbel A, Grange P, Colin JM (2002) Catal Today 75:113–117
30. Hermosin MC, Pavlovic J, Ulibarri MA, Cornejo J (1996) Water Res 30:171
31. Qian M, Zeng HC (1997) J Mater Chem 7:493–499
32. Xu ZP, Zeng HC (1998) J Mater Chem 7:2499–2506
33. Ambrogi V, Fardella G, Grandolini G, Perioli L (2001) Int J Pharam 220:23–32
34. Thevenot F, Szymanski R, Chaumette P (1989) Clays Clay Minerals 37:396–402
35. Tsuji M, Mao G, Yoshida T, Tamaura Y (1993) J Mater Res 8:1137
36. Chisem IC, Jones W (1994) J Mater Chem 4:1737–1744
37. Hibino T, Yamashita Y, Kosuge K, Tsunashima A (1995) Clays Clay Minerals 43: 427–432
38. Kooli F, Rives V, Ulibarri MA (1995) Inorg Chem 34:5122–5128
39. Kannan S, Swamy CS, (1997) J Mater Sci 32:1323–1630
40. Rey F, Fornes V, Rojo JM (1992) J Chem Soc Faraday Trans 88:2233
41. Hansen HCB, Koch CB, Taylor RM (1994) J Solid State Chem 113:46–53
42. Manna A, Imae T, Aoi K, Okada M, Yogo T (2001) Chem Mater 13:1674–1681
43. Carlino S (1997) Solid State Ionics 98:73–84
44. Ookubo A, Ooi K, Hayashi H (1993) Langmuir 9:1418–1422
45. Yun SK, Pinnavaia T (1995) J Chem Mater 7:348
46. Prosa TJ, Bauer BJ, Amis IJ (2001) Macromolecules 34:4897–4906
47. Li X, Imae T, Leisner D, López-Quintela MA (2002) J Phys Chem 106:12170–12177
48. Itoh, T, Ohta N, Shichi T, Yui T, Takagi K (2003) Langmuir 19:9120–9126